Wei-Che Chiu
Department of Biomedical Engineering,
Stony Brook University,
Stony Brook, NY 11794-8151

Gaurav Girdhar
Department of Biomedical Engineering,
Stony Brook University,
Stony Brook, NY 11794-8151

Michalis Xenos
Department of Biomedical Engineering,
Stony Brook University,
Stony Brook, NY 11794-8151

Yared Alemu
Department of Biomedical Engineering,
Stony Brook University,
Stony Brook, NY 11794-8151

Jõao S. Soares
Department of Biomedical Engineering,
Stony Brook University,
Stony Brook, NY 11794-8151

Shmuel Einav
Department of Biomedical Engineering,
Stony Brook University,
Stony Brook, NY 11794-8151

Marvin Slepian
Department of Biomedical Engineering,
Stony Brook University,
Stony Brook, NY 11794-8151;
Sarver Heart Center,
University of Arizona,
Tucson, AZ 85724

Danny Bluestein[1]
Department of Biomedical Engineering,
Stony Brook University,
Stony Brook, NY 11794-8151
e-mail: danny.bluestein@stonybrook.edu

Thromboresistance Comparison of the HeartMate II Ventricular Assist Device With the Device Thrombogenicity Emulation-Optimized HeartAssist 5 VAD

Approximately 7.5×10^6 patients in the US currently suffer from end-stage heart failure. The FDA has recently approved the designations of the Thoratec HeartMate II ventricular assist device (VAD) for both bridge-to-transplant and destination therapy (DT) due to its mechanical durability and improved hemodynamics. However, incidence of pump thrombosis and thromboembolic events remains high, and the life-long complex pharmacological regimens are mandatory in its VAD recipients. We have previously successfully applied our device thrombogenicity emulation (DTE) methodology for optimizing device thromboresistance to the Micromed Debakey VAD, and demonstrated that optimizing device features implicated in exposing blood to elevated shear stresses and exposure times significantly reduces shear-induced platelet activation and significantly improves the device thromboresistance. In the present study, we compared the thrombogenicity of the FDA-approved HeartMate II VAD with the DTE-optimized Debakey VAD (now labeled HeartAssist 5). With quantitative probability density functions of the stress accumulation along large number of platelet trajectories within each device which were extracted from numerical flow simulations in each device, and through measurements of platelet activation rates in recirculation flow loops, we specifically show that: (a) Platelets flowing through the HeartAssist 5 are exposed to significantly lower stress accumulation that lead to platelet activation than the HeartMate II, especially at the impeller-shroud gap regions (b) Thrombus formation patterns observed in the HeartMate II are absent in the HeartAssist 5 (c) Platelet activation rates (PAR) measured in vitro with the VADs mounted in recirculation flow-loops show a 2.5-fold significantly higher PAR value for the HeartMate II. This head to head thrombogenic performance comparative study of the two VADs, one optimized with the DTE methodology and one FDA-approved, demonstrates the efficacy of the DTE methodology for drastically reducing the device thrombogenic potential, validating the need for a robust in silico/in vitro optimization methodology for improving cardiovascular devices thromboresistance. [DOI: 10.1115/1.4026254]

1 Introduction

The number of patients suffering from cardiovascular diseases grows annually, and approximately 2% of the United States population ($\sim 5.7 \times 10^6$) are diagnosed with congestive heart failure (CHF) with a projected 25% of increase in their number by 2030 [1]. Mechanical circulatory support (MCS) devices, such as total artificial hearts (TAHs) or ventricular assist devices (VADs) were introduced as a bridge-to-transplant (BTT) to sustain eligible patients while waiting for available heart transplants [2,3]. Owing to insufficient amount of eligible organs for heart transplant annually [4], the Food and Drug Administration (FDA) approved the use of one of the more hemodynamically and mechanically robust VADs, the Thoratec HeartMate II VAD (HMII; Thoratec Corp., Pleasanton, CA), for destination therapy in 2010 [5,6].

Prior to the HeartMate II, various VADs were developed and introduced to the market broadly under the following two categories: pulsatile-flow (i.e., the first generation pulsatile VADs) and continuous-flow (i.e., the second generation axial VADs and the third generation centrifugal VADs) [7,8]. Due to their relatively simpler mechanics, the continuous-flow VADs provide higher durability and require smaller implantation volume than the pulsatile-flow VADs. In the continuous-flow VADs, the blood is constantly propelled out from the apex of the left ventricle by a turbine, and returned to the ascending aorta. In order to generate physiological cardiac outputs, those continuous-flow VADs operate at very high impeller speeds (7000 to 12,000 RPM), which generates unusually high shear stress levels in some locations like the impeller-shroud gaps and regions of elevated residence time in the rear (inlet) and front (outlet) hubs. These high stress accumulation regions may potentially cause damage to the blood cells flowing through the device (e.g., hemolysis of RBCs and activation of platelets has been reported) [9,10], which may lead to various post-implant complications, such as flow-induced platelet

[1]Corresponding author.
Contributed by the Bioengineering Division of ASME for publication in the JOURNAL OF BIOMECHANICAL ENGINEERING. Manuscript received September 8, 2013; final manuscript received December 10, 2013; accepted manuscript posted December 16, 2013; published online February 5, 2014. Editor: Victor H. Barocas.

activation, aggregation, and subsequent thromboembolic complications or complete device obstruction/malfunction due to thrombus formation [11–14]. Due to these post-implant complications, device recipients are mandated to life-long antiplatelet and anticoagulation regimens, which lead to secondary complications such as heparin-induced thrombocytopenia or several bleeding incidents [15–18]. In order to reduce or eliminate the administration of the antiplatelet or anticoagulation regimens, modifying the geometrical features of the VADs implicated in higher stress accumulation by applying the device thrombogenicity emulation (DTE) methodology in order to reduce the device thrombogenic potential has shown to be a very promising approach, and is briefly described below [11,19,20].

Our group had successfully optimized the thrombogenic performance of an axial continuous-flow VADs, the modern MicroMed DeBakey VAD (DeBakey; MicroMed Cardiovascular, Inc., Houston, TX). The optimized version of the device called MicroMed HeartAssist 5 VAD (HA5; MicroMed Cardiovascular, Inc., Houston, TX) shows an order of magnitude reduction in flow-induced thrombogenicity in vitro [11] and markedly improved benefit over Aspirin or Dipyridamole addition in vitro [20]. The DTE methodology interfaces numerical (in silico) flow simulations with in vitro experiments performed in a hemodynamic shearing device (HSD), which replicates stress-time data extracted from problematic regions of the device, to perform iterative optimization of the device thrombogenic potential [11,19,21]. This in silico/in vitro methodology can potentially reduce the research and development costs of developing thromboresistant mechanical circulatory support (MCS) devices by reducing the need for costly in vivo experimentation prior to the device approval by the FDA. As mentioned previously, the HMII is currently the only FDA approved continuous-flow VAD for both BTT and DT—it has been widely implanted worldwide [2,3,5,6]. However, HMII recipients still require long-term/life-long anticoagulation or antiplatelet regimens, yet not eliminating post-implant bleeding or thrombotic complications [17,22,23]. For instance, in approximately 6% of HMII recipients' device thrombosis was reported which lead to replacement of the implanted device with associated morbidities [12–14,24]. Given this high incidence of thrombotic complications rates, it is judicious to compare this FDA-approved VAD (HMII) currently in clinical use with a similar device which thrombogenicity has been optimized such as the HA5 VAD [11].

The weight of HMII is approximately 3-fold that of HA5 (i.e., 281 g compared to 92 g, respectively), with approximately 2.3-fold larger external volume (i.e., approximately 117,628 mm^3 and 50,187 mm^3 of HMII and HA5, respectively) (Figs. 1(*a*)*i* and (*b*)*ii* for HMII and HA5, respectively). Due to the smaller dimension and lighter weight, the HA5 offers significant benefits of implanting the HA5 in the pericardial space while the HMII has to be implanted below the diaphragm. Due to the design differences of the interior components between these two VADs, the HA5 has slightly larger fluid volume capacity than the HMII (5.55 ml and 5.80 ml of fluid in the HMII and HA5, respectively, from the inlet tip of the flow straightener to the exit tip of the diffuser (Figs. 1(*a*)*ii* and (*b*)*ii* for HMII and HA5, respectively)). This implies that the HA5 may consume less energy and operate at a lower impeller speed—to generate identical cardiac output (CO) as compared to the HMII.

In the present study, we compared the thromboresistance of the DTE-optimized HA5 VAD with that of the FDA-approved HMII VAD—both numerically and experimentally. In the numerical simulations, we extracted and compared the probability density function (PDF; serves as the "thrombogenic footprint" of the device) of the stress accumulation (SA) of large number of platelets flowing through both VADs. We also performed device in vitro flow-loop experiments under physiologically representative conditions and measured the shear-induced platelet activation rates (PAR) of both VADs with recirculating human purified platelets. We then identified thrombus-prone locations from prior clinical studies in the HMII (explanted VADs) and utilized results from our numerical simulations to extract stress-time trajectories for individual platelets exposed to those locations to explain the clinical findings of the thrombus formation patterns observed in the HMII [12–14].

2 Materials and Methods

2.1 Ventricular Assist Devices. Extensive numerical simulations were conducted in the two VADs: Thoratec HeartMate II (HMII, Fig. 1(*a*)*i*); Thoratec Corp., Pleasanton, CA) and MicroMed HeartAssist 5 (HA5, Fig. 1(*b*)*i*); MicroMed Inc., Houston, TX). In axial turbine design blood pumps, the blood flowing through axial VADs is driven by the rotational impellers, which are actuated by electromagnetic motors as shown in the Figs. 1(*a*) and 1(*b*). As mentioned previously, the HA5 is the optimized design of the modern DeBakey VAD with the following specific design modifications—the four original orthogonal flow straightener blades were replaced with three blades design, 120 deg apart, the rear (inlet) and front (outlet) hubs had been streamlined, and the impeller blade leading edge, profiles, length, pitch and pitch-angle were modified [11]. While both HMII and HA5 share overall similar design features, they differ in their design as marked in the Figs. 1(HMII: (*a*)*ii*; HMII: (*b*)*ii*:) (A) The flow straighteners consist of three stationary blades, 120° radially apart, straightening the incoming blood flow along the axial direction. Numerous twisted magnetic impeller blades attach on the impeller surfaces of each VAD (3 and 6 impeller blades for HMII and HA5, respectively). (B) A marked difference in the design of the two devices is the spinning direction of their impellers: counterclockwise and clockwise directions for HMII and HA5, respectively. (C) Downstream of the impellers both VADs have a stationary diffuser, which incorporates numerous twisted diffuser blades (HMII and HA5 have 3 and 6 diffuser blades, respectively) to redirect the blood outflow from the circumferential direction back to the axial direction while exiting the devices.

2.2 Numerical Simulation of Flow Through VADs. The thrombogenic potential of both VADs were numerically computed using fluid structure interaction (FSI) simulations incorporating two-phase flow consisting of a particulate phase (platelets) suspended in blood flowing through the VADs under constant cardiac output of 4 L/min. Highly refined meshes were generated with the commercial mesh generator Gambit (Ansys Fluent Inc., Lebanon, NH). Studies of mesh independence were conducted with various mesh densities for each VAD—9, 13 and 19×10^6 elements for the HA5, and 12, 13 and 17×10^6 elements for the HMII. After establishing mesh independence in both VADs numerical meshes, an optimized grid density of $\sim 9 \times 10^6$ elements was determined for the HA5 and $\sim 17 \times 10^6$ elements for the HMII. These numerical flow simulations were computed using parallel processing via a multiprocessor Linux server (OS: CentOS 6.4) using up to 30 cores, and the eventual simulation time for each flow simulation was approximately four months.

The FLUENT CFD solver (Ansys Fluent Inc., Lebanon, NH) was utilized for conducting fluid structure interaction (FSI) simulations, with the rotating impellers propelling the blood through the VADs, using the two equation k-ω turbulence model for solving unsteady Reynolds averaged Navier-Stokes (URANS) for 30 and 27 impeller revolutions for the HMII and HA5, respectively [11]. Blood was modeled as two-phase Newtonian fluid with viscosity of 0.0035 kg/m-s and density of 1081 kg/m^3, with platelets assumed as neutrally buoyant solid 3 μm diameter spherical particles (density: 998.2 kg/m^3). This two-phase flow model takes into account the particle-fluid interactions (drag, lift and Basset

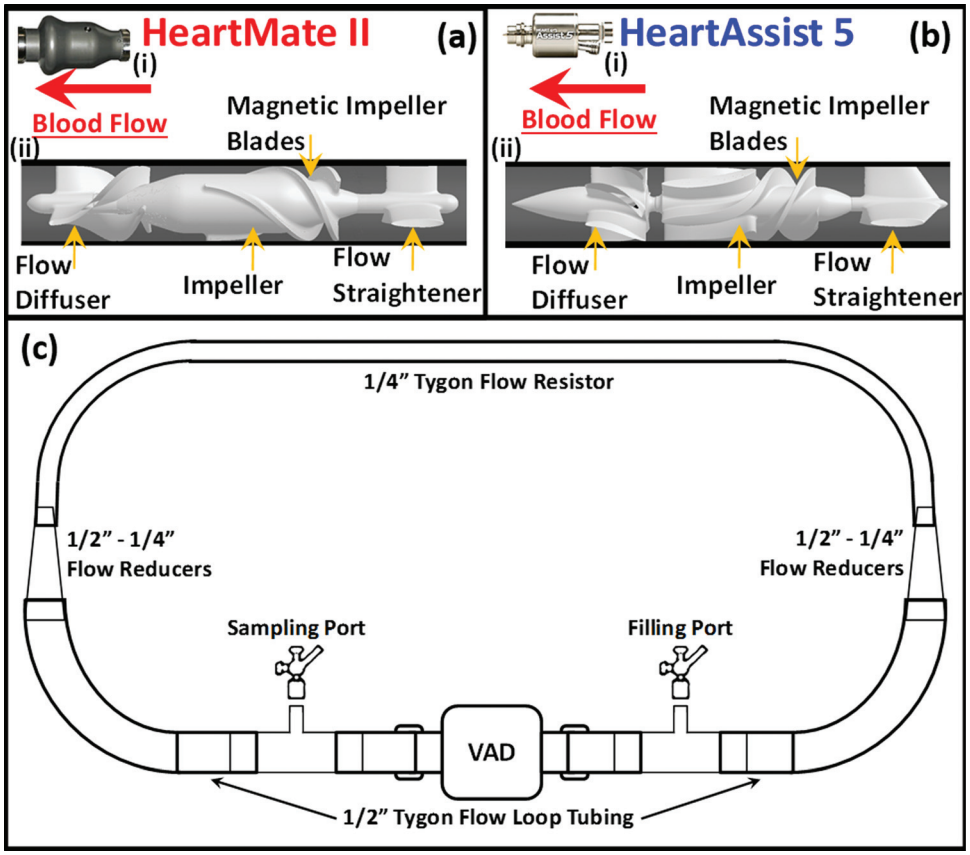

Fig. 1 Illustrations of the exterior and interior features of (*a*) HMII and (*b*) HA5 and (*c*) Flow-loop for the in vitro experiments. The exterior features of HMII (*a*)*i* and HA5 (*b*)*i*; the length of the VADs are 71 mm and 81 mm, and the maximum diameter are 30 mm and 43 mm for HA5 and HMII, respectively. The interior features and the detailed components of HMII (*a*)*ii* and HA5 (*b*)*ii*; both VADs share similar overall design, which encloses the stationary flow straightener and diffuser, a single rotational impeller—both impellers actuated via electromagnetic fields. The flow straighteners for both VADs are composed of three blades, 120 deg apart. The spinning direction of the impeller of HMII and HA5 are opposite. 90 ml of flow-loops (*c*) were assembled for the in vitro experiments, consisting of two tube segments with inner diameter of 1/2" connected to the VADs, and a segment of flow-resistor-tube, with the inner diameter of 1/4", was connected to the flow-tubes with two tapered flow reducers, combining in series two reducing connectors (1/4"–3/8" and 3/8"–1/2").

forces, as well as turbulent fluctuations), as previously described [11,25]. The volumetric mesh elements surrounding the impeller region of both VADs were modeled as rotational volumetric mesh with its axis aligned along the flow direction. The volumetric meshes at the other regions of both VADs' geometries were modeled as stationary meshes. Mesh interfaces were applied on the surfaces between the moving and stationary meshes (Fig. 2(*a*)*i* and 2(*b*)*i* for HA5 and HMII, respectively). The rotational direction and speed of the impeller of each VAD were set (HMII: 10,000 RPM, counterclockwise; HA5: 9000 RPM, clockwise) corresponding to the operating conditions of each VAD when implanted in patients so that both VADs generate the same physiological CO of 4 L/min. These parameters, i.e., RPM and CO, also correspond to the operating conditions of the VADs in the in vitro recirculation experiments (described later). Mass flow rate of 0.07 kg/s (corresponding to this CO) was applied at both VADs as the inlet boundary condition, and outlet pressure boundary condition applied initially at 0 Pa. Approximately 32,000 and 31,000 platelets were seeded at the upstream planes of the HA5 and HMII, correspondingly (Fig. 2(*a*)*ii* and 2(*b*)*ii* for HA5 and HMII, respectively). An optimized time step of 7×10^{-5} s was determined for both VADs as previously described [11], resulting in the corresponding degrees of the rotating rotor position per time step of 3.78 and 4.2 degrees for HA5 and HMII, respectively. Approximately 90% of the platelets have a residence time of less than 184 ms while flowing through the VADs. The stress loading history of the platelet trajectories flowing through these VADs—stress accumulation (SA), were computed by incorporating the combined effect of shear stress and exposure time. In order to take into account the contribution of both the viscous and turbulent stresses (τ_{ij}) in the SA formulation, we adapt a formulation for blood damage (platelet activation) which is based on a comparative stress theory and is formulated for fluids in analogy to the von Mises yield criterion from damage theory for solid materials [26,27]. It considers the six components of the general stress tensor, circumventing the issue of estimating directly the contribution of the turbulent Reynolds stresses by rendering the contribution of all the stress components of the stress tensor into a scalar which represents their contribution in an average sense. This is a common approach for estimating blood damage in turbulent flows. Similar approaches were previously applied by many other groups [28], as well as in many of our previous studies of platelet activation in devices [19,21]. The stress tensor extracted from the simulation along the corresponding trajectories was rendered accordingly into a scalar stress value (σ) [26,27] as follows:

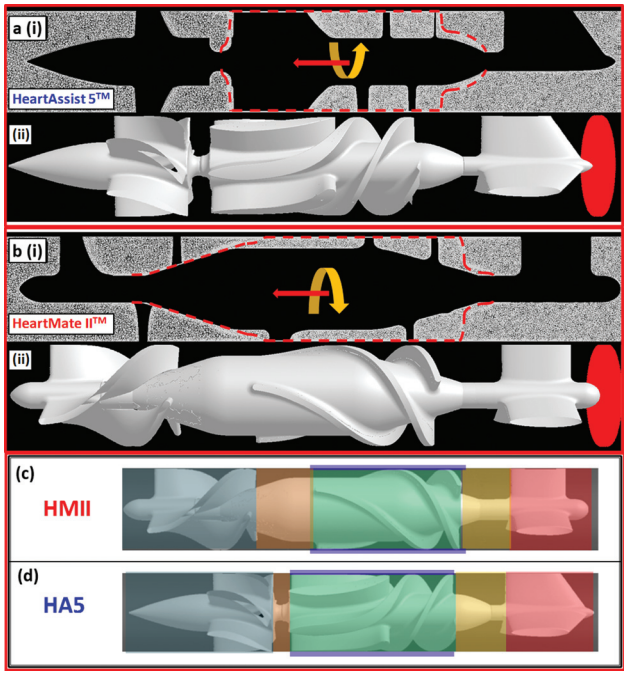

Fig. 2 Illustrations of mesh elements and the seeded platelet particles for the simulations of HA5 (*a*) and HMII (*b*) and the ROIs' definitions of HMII (*c*) and HA5 (*d*)- (*a*)*i* and (*b*)*i* indicates the side views of the volume meshes of the HeartAssist 5 (HA5) and HeartMate II (HMII) simulations, and the red dashed line indicates the mesh interfaces between the stationary and moving volume meshes. The HA5 mesh had approximately 9.3×10^6 elements, and the HMII mesh had approximately 17×10^6 elements. The yellow arrows indicate the spinning direction of the moving volume meshes, and the red arrows indicate the flow direction for both VADs- the HA5 spins clockwise along the flow, while the HMII spins counterclockwise. (*a*)*ii* and (*b*)*ii* approximately 31,000 and 32,000 platelets (red particles) were seeded and released from the upstream of the HA5 and HMII, accordingly. (*c*) and (*d*) six different ROIs were defined for both VADs (i.e., flow straightener ROI (red), rear hub ROI (yellow), impeller-shroud gap ROI (purple), impeller blade ROI (green), front hub ROI (orange), and diffuser ROI (navy blue)). The flow straightener ROI was defined from the entry tip to the tail of flow straightener blades as cylinder. The rear hub ROI was defined as the cylindrical area from the tail of the flow straightener blades to the head of impeller blades. The impeller-shroud gap ROI was defined as the annular area between the tip of the impeller blades and the shroud. The impeller blade ROI was considered as the area between each impeller blades. The front hub ROI covered the cylindrical area from the tail of impeller blades to the head of the diffuser blades. The cylindrical area from the head of the diffuser blades to the exit tip of the diffuser was defined as the diffuser ROI.

$$\sigma = \frac{1}{\sqrt{3}} \times \sqrt{\tau_{11}^2 + \tau_{22}^2 + \tau_{33}^2 - \tau_{11}\tau_{22} - \tau_{11}\tau_{33} - \tau_{22}\tau_{33} + 3(\tau_{13}^2 + \tau_{23}^2 + \tau_{13}^2)}$$

The SA is computed by the summation of the linear product of this scalar stress (σ) and the exposure time (t_{exp}) which were extracted from each platelet trajectory [21,29] as follows:

$$SA = \sigma \times t_{exp} = \int_{t_0}^{t_{exp}} \sigma(t)dt = \sum_{i=1}^{N} \sigma_i \times \Delta t$$

where σ_i, $i = 1, 2, \ldots, N$, is the nodal scalar value extracted from the total stress tensor and Δt is the corresponding time step between successive nodal points.

The large number of stress accumulation (SA values) reached by each platelet along their corresponding trajectories while flowing through each VAD were collapsed into a probability density functions (PDF) to statistically represent the distribution of the SA of all trajectories in each VAD (the "thrombogenic footprint"). This facilitated the comparison between the two VADs. The comparisons were focused on two ranges of the PDF—the main mode and the tail region. The main mode of PDF represents the mean SA value for most of the trajectories flowing through the device (bulk flow), and the tail region represents the distribution of the trajectories at the higher and riskier SA range, which is prone to activate the platelets. The PDF comparisons for the two specific SA brackets (i.e., the main mode and the tail regions) were additionally performed at specific regions of interest (ROIs), as well as for the complete device for both the HA5 and HMII.

The PDFs for both VADs and for specific ROIs (specific ROIs corresponding to the flow straightener, inflow bearing, impeller-shroud gap, impeller blades, outflow bearing, and the diffuser (Figs. 2(*c*) and 2(*d*) for HMII and HA5, respectively)) were computed with an in-house C++ code that calculated the SA of the platelets in each ROI. The inflow and outflow bearing ROIs were defined as the regions between the blades of flow straightener, impeller and diffuser. The impeller blades ROI is defined by the region between the impeller blades, and the impeller-shroud gap ROI is defined as the annular region between the tip of the impeller blades and the shroud.

2.3 Numerical Prediction of Thrombus Formation. From prior clinical observations in the explanted HMII VADs, device thrombosis occurred most commonly at the rear hub region and along the flow straightener blades [12–14,30]. An in-house code was used for analyzing the platelet trajectories extracted from both VADs simulations at these hub regions. The locations of the specific platelet trajectories were identified based on the elevated residence time of the trajectories.

2.4 In Vitro Platelet Activation Measurements in Recirculation Flow-Loops. Both VADs were mounted in recirculation flow loops to generate the target physiologic cardiac output of 4 L/min, corresponding to impeller speeds of 9000 and 10,000 RPM for the HA5 and HMII, respectively, and the pressure head (ΔP), as illustrated in Fig. 1(*c*). The cardiac output of 4 L/min was chosen based on the most common clinical operating conditions for both devices. The impeller speeds for each VAD was determined according to the respective operating conditions required for generating the designated cardiac output of 4 L/min when mounted in the flow-loop. The flow-loops consisted of two Tygon R3603 tubes connected as follows: (1) the 0.5 in. ID flow tubes for connecting the VAD, and (2) 21 in. long and 0.25 in ID flow resistor tubing for generating a semiphysiological pressure rise across the pump of ~70–80 mmHg. (3). the 0.5 in VAD connecting flow tubes and 0.25 in central flow resistor tubing were connected with two tapered 0.5 in—0.25 in reducing connectors, which were formed by adding in series two additional reducing connectors 0.5 in to 0.375 in and 0.375 in to 0.25 in (NovoSci, Conroe, TX) to avoid the sudden reduction or expansion of flow with the transition to the flow resistor. The total volume of the flow-loop, including the VADs, was 90 ml.

2.5 Platelet Activation Measurements. Citrated blood (120 ml) was obtained from healthy adult volunteers ($n = 10$) who have abstained from all medication, including aspirin, for at least two weeks prior to blood donation, after obtaining written and informed consent (protocol approved by Stony Brook University IRB) prior to venipuncture. Gel-filtered platelets were prepared and diluted to a concentration of $15 \times 10^3/\mu l$ with modified Tyrode's buffer. 90 ml of platelets-buffer solution was recirculated in the flow-loop for 30 min as previously described [11]. The in vitro experiments in the HMII and HA5 VADs were performed

Table 1 Mean (±SD) of stress accumulation (SA) for platelet trajectories flowing through regions of interest (ROIs) in the HMII and HA5 VADs

ROIs	HeartMate II *SA* (dyne-s/cm^2)	HeartAssist 5 *SA* (dyne-s/cm^2)
OverallVAD	13.362 ± 15.887	12.997 ± 12.418
Flow Straightener	0.694 ± 2.213	0.838 ± 2.742
Rear Hub Bearing	0.58 ± 1.183	0.779 ± 1.659
Impeller-ShroudGap	20.598 ± 16.052	9.455 ± 11.882
Impeller Blades	2.694 ± 3.316	2.858 ± 2.058
Front Hub Bearing	2.051 ± 4.142	1.047 ± 1.332
Flow Diffuser	3.535 ± 5.074	3.603 ± 5.927

simultaneously using the same platelet batches. Thrombogenicity of both VADs was measured in timed samples extracted from the recirculation flow-loops at t = 0, 10, 20, and 30 min, with our well established platelet activity state (PAS) assay [31]—which uses acetylated prothrombinase to prevent the positive feedback of thrombin for further activating platelets; thus offering a 1:1 correspondence with the agonist (shear stress). The platelet activity state was normalized in respect to the maximum thrombin generation of fully-activated platelets (achieved by sonicating the platelets) and reported at each time point for both VADs. The linear fitted slopes of the normalized PAS from timed samples represent the platelet activation rates (PAR) during the 30 min experiments. A student's t-test was utilized to statistically analyze the differences of the PARs between both VADs, as previously described [11].

3 Results

3.1 Overall Stress Accumulation (SA) for HA5 and HMII from the Numerical Simulations. The global PDFs of HMII and HA5 VADs showed the following: (A) The main SA modes of both VADs populated a similar range—the mean SA for HMII and HA5 was 13.362 ± 15.887 dyn sec/cm^2 and 12.997 ± 12.418 dyn sec/cm^2, respectively (Table 1); (B) Comparing the distribution of the SA at the tail regions of the PDFs indicated that platelets flowing through HMII have significantly higher probability to be exposed to a higher SA (range between 50–100 dynes sec/cm^2) than the HA5 (Fig. 3, inset). The mean SA in the tail region was 62.572 ± 14.659 dynes sec/cm^2 and 60.711 ± 25.588 dyn sec/cm^2 for HMII and HA5, respectively.

3.2 Regions Specific (ROI) SA From the Numerical Simulations. The PDFs of both VADs at the flow straightener ROI populated a similar low SA range (Table 1; mean SA: 0.694 ± 2.213 and 0.838 ± 2.742 dynes sec/cm^2 for HMII and HA5, respectively) with a similar SA distribution of the PDFs' tail regions—the higher SA range (Fig. 4(*a*); inset, range between 1–60 dynes sec/cm^2). The PDFs of the rear hub bearing ROI populated a similar low SA range for both VADs (Table 1; mean SA: 0.58 ± 1.183 and 0.779 ± 1.659 dynes sec/cm^2 for HMII and HA5, respectively); however, higher density value of the high SA was found the tail region PDF of the HMII as compared to the HA5 at this ROI (Fig. 4(*b*); inset, range between 10–50 dynes sec/cm^2). Compared to the main mode of the HMII PDF at the impeller-shroud gap ROI, the main mode of the HA5 PDF at this ROI was shifted to the left toward the lower SA range. (Table 1; mean SA: 20.598 ± 16.052 and 9.455 ± >11.882 dynes sec/cm^2 for HMII and HA5, respectively), and the distributions at the tail region PDF indicated higher probability for platelets flowing through HMII to be exposed to elevated SA (Fig. 4(*c*); inset, range between 10–110 dynes sec/cm^2).

The PDFs of both VADs at the impeller blade ROI populated a similar low SA range (Table 1; mean SA: 2.694 ± 3.316 and 2.858 > ± 2.058 dynes sec/cm^2 for HMII and HA5, respectively);

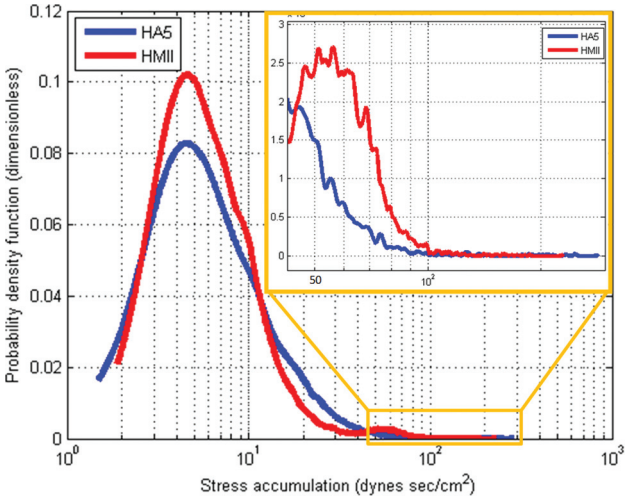

Fig. 3 PDF Results from the Overall Devices of HMII and HA5-The PDF results of the overall regions of HMII and HA5 populated a similar slow SA range of both VADs; however, the distribution of the tail region (riskier high SA) showed higher thrombogenic potential in the HMII

however, according to the distribution of the tail region PDF of this ROI, higher density of high SA was found in the HMII comparing to the HA5 (Fig. 4(*d*); inset, range between 10–100 dynes sec/cm^2). The PDF of the outflow bearing ROI indicated that the main mode of the HMII is right shifted toward higher SA range as compared to the HA5 (Table 1; mean SA: 2.051 ± 4.142 and 1.047 ± 1.332 dynes sec/cm^2 for HMII and HA5, respectively); furthermore, the tail region PDFs indicated an higher probability of platelets being exposed to elevated SA for the HMII (Fig. 4(*e*); inset, range between 40–110 dynes sec/cm^2). The main mode of the HMII at the diffuser ROI was left shifted toward a lower SA as compared to that of the HA5 (Table 1; mean SA: 3.535 ± 5.074 and 3.603 ± 5.927 dynes-sec/cm^2 for HMII and HA5, respectively). However, both VADs had similar distributions of SA at their tail regions PDF (Fig. 4(*f*); inset, range between 10–120 dynes sec/cm^2) at this ROI.

3.3 Mapping Thrombus-Prone Regions in the HMII and HA5 From the SA Data. In the HMII, numerous platelet trajectories with significant recirculation portions (i.e., prolonged exposure time) were found at the downstream of the flow straightener blades, with an average eddy radius of approximately 2 mm. Also, several stagnant platelets resided nearby the rear hub bearing (Fig. 5(*a*)). Furthermore, some platelets were found to be trapped at the entry of the impeller blades, moving along with the rotational motion of the impeller but not escaping from this region (Fig. 5(*b*)). Conversely, in the HA5 in a similar ROI, no platelet trajectories were observed to recirculate downstream of the flow straightener and the rear hub bearing, and very few stagnant platelet trajectories were found at the rear hub bearing (Fig. 5(*c*)). No trapped platelets were found at the entry of the impeller blades (Fig. 5(*d*)).

3.4 Platelet Activation Measurements in Flow-Loop Experiments. Platelets were recirculated in the flow-loop with the VADs operating at 4 L/min CO, and measurements of platelet activation state (PAS) were conducted at specific time-points, as described above. A linear-fit of the PAS over time yielded the slope of the PAS, i.e., the platelet activation rate (PAR). The results from the 30 min in vitro experiments showed that the PAR of the HA5 was approximately 2.5-fold lower than that of the HMII—(Figs. 6; $4 \times 10^{-5}\,\text{min}^{-1}$ and $1 \times 10^{-4}\,\text{min}^{-1}$ for the HA5 and the HMII, respectively; $p < 0.05$). This corroborated the numerical simulation results with PDFs clearly showing a much

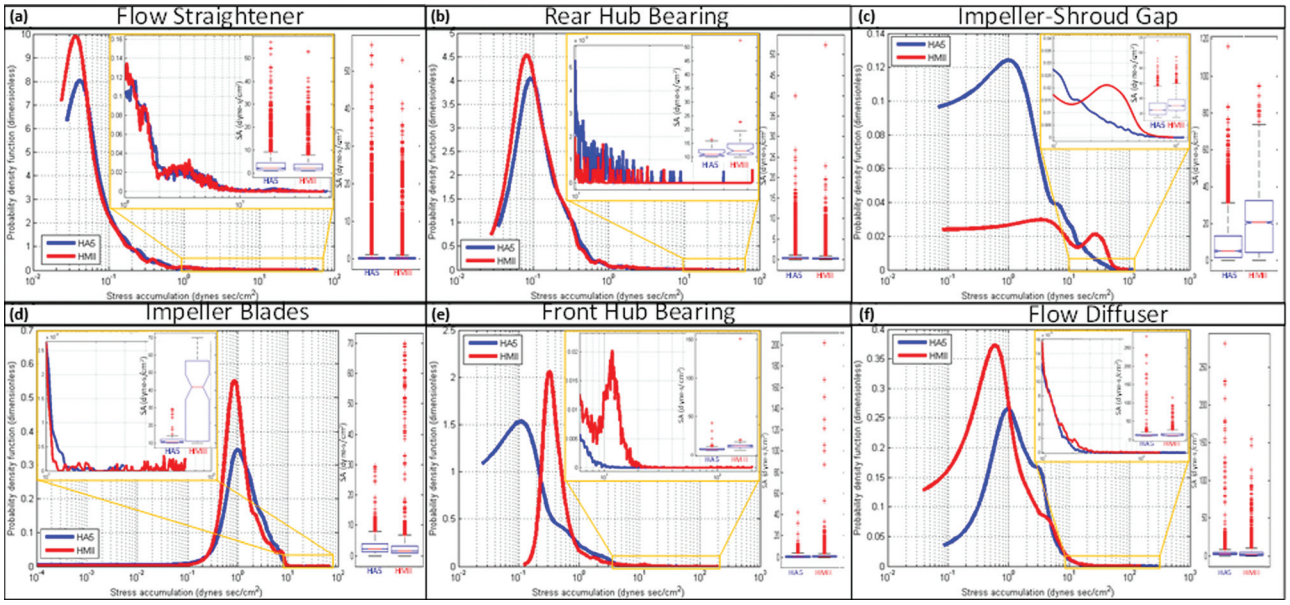

Fig. 4 PDF Results at ROI regions—PDF results obtained from the flow straightener ROI populated a similar low SA range in both VADs, and similar tail region distributions were found. The PDF results from the rear hub ROI populated a similar low SA range between two VADs; however, higher probability density (thrombogenic potential) was found at the HMII tail region comparing to the distribution of the HA5 tail region. Very different PDF distributions between the HMII and HA5 were found at the impeller-shroud gap ROI; the main mode of the HA5 is left-shifted (toward lower SA range) compared to the HMII, and higher distribution at the HMII tail region (riskier high SA range) comparing to the HA5. PDF results from the impeller blade ROI indicated that the main modes of both VADs populated a similar low SA range; however, the tail region of HMII's PDF showed higher density at higher SA range than the HA5. The PDF results from the front hub ROI showed that the main mode of HMII was right-shifted (toward higher SA range) comparing to HA5's main mode, and an additional mode was observed at the tail region of HMII comparing to HA5. The PDF result from the diffuser ROI indicated the main mode of HA5 was right-shifted compared to HMII, but very similar distribution was found at the tail region of both VADs.

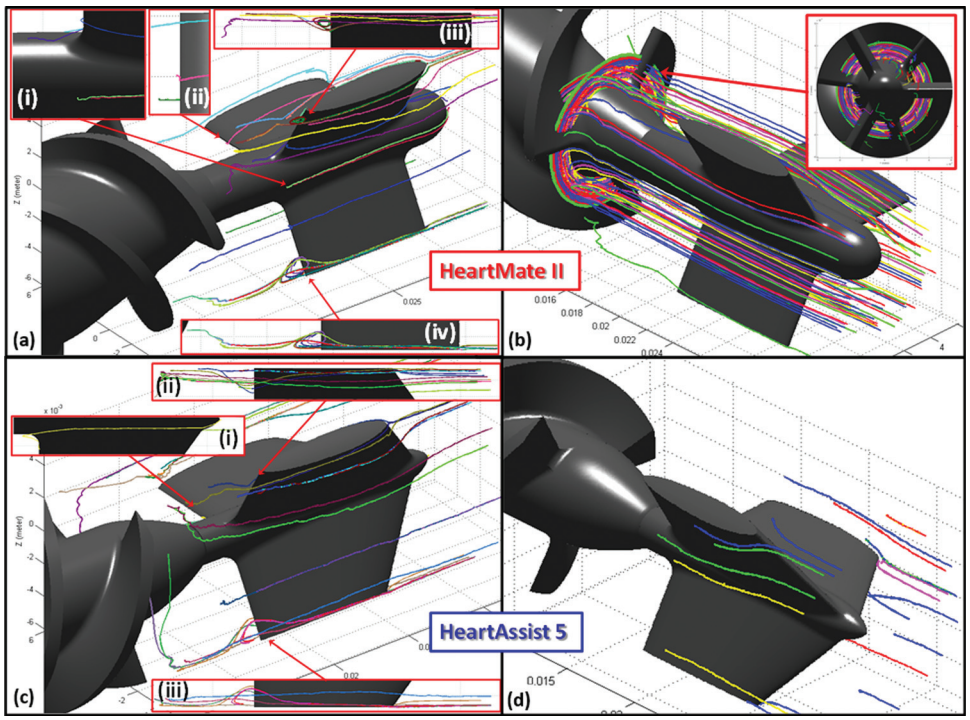

Fig. 5 Stagnant platelet trajectories and recirculation zones in HMII and HA5- (*a*) The recirculation zones and stagnant platelet trajectories were observed at the downstream of the flow straightener blades of HMII, with approximately 2 mm of the average eddy diameter. (*b*) Several entrapped platelet trajectories were observed at the entry of the impeller blades of the HMII, and closely following the rotational motion of impeller. (*c*) Fewer stagnant trajectories were observed at the rear hub region of the HA5 comparing to the HMII, and no recirculation zone was found. (*d*) No entrapped platelet trajectory was observed at the entry of the HA5 impeller. These platelet trajectories were represented as a time average of their residence time (184 ms).

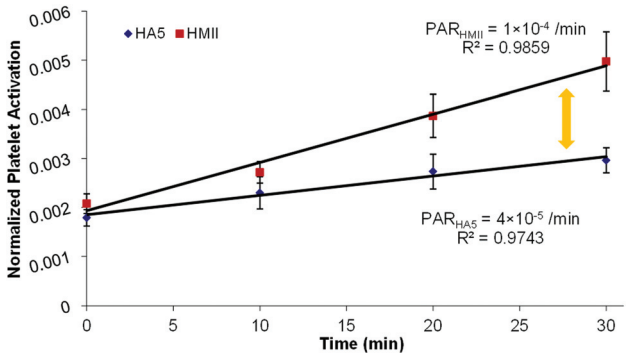

Fig. 6 2.5-fold differences of the thrombogenicity between HMII and HA5- The platelet activation rates (PARs) of HMII (red) and HA5 (blue) after 30 min flow-loop experiments indicated significant 2.fivefold differences. The PARs of HMII and HA5 were 1×10^{-4}/min and 4×10^{-5}/min, accordingly ($p < 0.05$; $n = 10$).

higher probability of platelets being exposed to elevated SA in the case of the HMII—correlating to the higher measured activation rate in the HMII.

4 Discussion

In the present study, we have compared the thrombogenic potential of the DTE-optimized Micromed HA5 and the FDA-approved Thoratec HMII. The comparison is based on both in silico simulations and in vitro experiments in which we have successfully demonstrated the ability to map the thrombogenic footprints of the two axial VADs (PDFs) (Fig. 3), map specific thrombogenic regions through ROI (regions of interest) comparisons (Fig. 4), map thrombus-prone regions in these two VADs (Fig. 5), and confirm the predictions of the numerical simulations with in vitro platelet activation measurements in recirculation flow loops (Fig. 6).

We showed here that platelets flowing through the HA5 VAD have less potential to be exposed to the riskier high stress accumulation range as compared to the HMII (Fig. 3). Specifically, the rear hub (inflow) bearing region, the impeller-shroud gap region, impeller blades regions and the front hub (outflow) bearing regions of the HA5 had lower thrombogenic potential as compared to the HMII (Figs. 4(*b*)–4(*f*))—the platelets flowing through these regions of HA5 have less probability to be exposed to the riskier high stress accumulation comparing to the platelets flowing through the same regions in HMII.

As mentioned earlier, pump thrombosis was reported in approx. 6% of the HMII recipients [24]. Most thrombus formation was observed at the downstream of the flow straightener blades and the entry region of the impeller blades [12–14,30]. These clinically reported regions matched the locations where numerous fluid recirculation zones, with several stagnant or entrapped platelet trajectories were observed from the HMII simulation (Figs. 5(*a*) and 5(*b*)). Although longer term clinical studies of the HA5 are currently not available, according to the numerical simulations we have conducted in the current study, much fewer stagnant platelet trajectories were found at similar regions as compared to the HMII, and no recirculation zones or trapped trajectories were observed (Figs. 5(*c*) and 5(*d*)), which indicated that the HA5 may

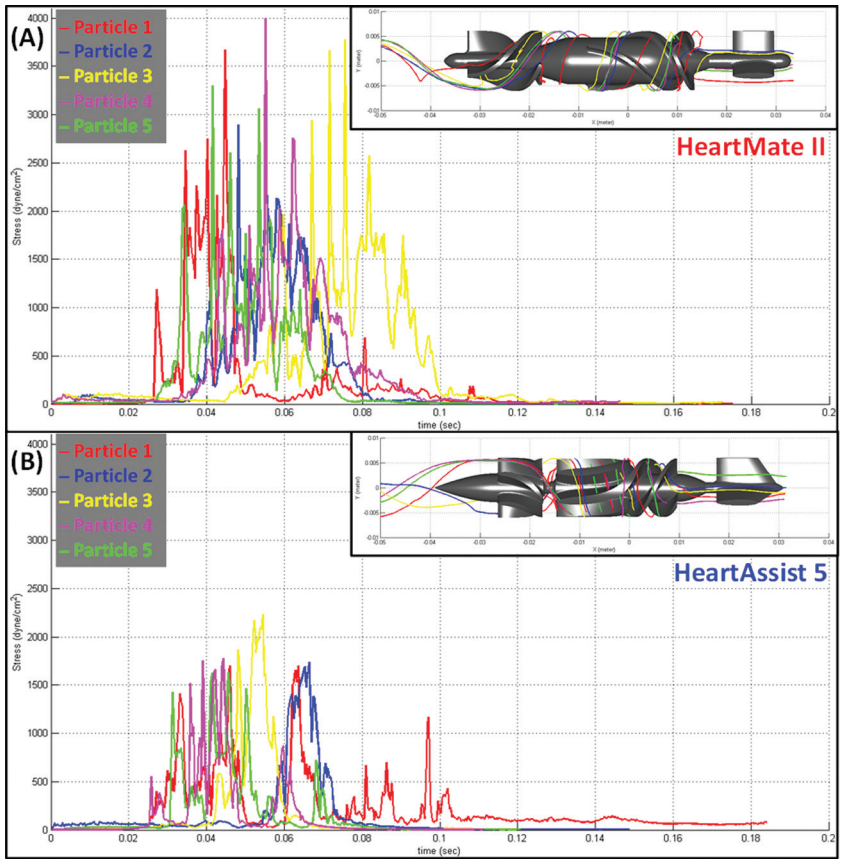

Fig. 7 Markedly lower stress accumulation of platelet trajectories flow through impeller-shroud gap of HA5 representative shear stress and exposure time of five platelet trajectories flow through the impeller-shroud gap of (*a*) HMII and (*b*) HA5 VADs are shown. The platelet trajectories flowing through the HA5 has lower shear stress magnitude and shorter exposure time comparing to the trajectories flowing through the HMII.

have less incidence of device thrombosis as compared to the HMII.

Confirming the predicted lower thrombogenic potential of the HA5 over the HMII described above, the platelet activation measurements performed in both VADs showed that the thrombogenicity of the HA5 was approximately 2.5-fold lower than that of the HMII (Fig. 6). Higher stress magnitude and longer exposure times characterizing the platelet trajectories flowing through the impeller-shroud gap region of the HMII (where the most significant difference was found in the ROI's PDFs as compared to the HA5) are clearly depicted in Fig. 7, showing the increased thrombogenic potential of the HMII for selected similar platelet trajectories of the two devices. Although the actual physiological loading conditions in which VAD operates in the body cannot be replicated in such a small volume recirculation flow loop (90 ml), it facilitates comparative measurements of platelet activation by different VAD designs using fresh blood donations while maintaining semi physiological CO and pressure head. In that, this in vitro recirculation flow loop serves as an excellent proxy for conducting comparative measurements of the thrombogenic potential of various VADs.

As mentioned earlier, although the HMII has been approved by the FDA for both bridge-to-transplant (BTT) and destination therapy (DT), several post-implant complications still remain (mostly due to device generated nonphysiological flow patterns which induce high shear stresses, and the secondary complications due to the complex pharmacological regimens the former mandate). Based on the present study, the HA5 offers not only an anatomical advantage because of its smaller dimension, but better thromboresistance, which may clinically translate into a significant reductionof the mandatory anticoagulation/antithrombotic drug regimen as compared to an FDA-approved VAD device which was not optimized with the DTE methodology as the HA5 was.

5 Conclusions

Advanced numerical simulations designed to evaluate the thrombogenic performance of blood recirculating devices were used to demonstrate the efficacy of the DTE methodology for optimizing the thromboresistance of a rotary VAD by comparing a DTE optimized VAD (HA5) to that of a FDA approved VAD (HMII) which was not optimized by DTE. The numerical simulations were further validated by comparing the platelet activity measured in the two VADs in an in vitro recirculation flow-loop. The numerical simulations clearly indicated that the HA5 VAD has a lower thrombogenic potential as compared to the HMII, with distinct advantages in specific regions that were the focus of the optimization. Furthermore, flow patterns leading to thrombus formation in the HMII were mostly absent in the optimized HA5. The in vitro recirculation studies conducted in the two VADs showed that the thrombogenicity of HA5 was 2.5-fold lower than that of the HMII. This study demonstrates the robust applicability of our DTE methodology for reducing the thrombogenicity of continuous flow rotary VAD designs. The same approach may be applied to any type of blood recirculating device and may obviate the need for the complex antithrombotic and anticoagulant management of patients implanted or treated by such devices.

Acknowledgment

This project was supported by grants from the National Institute of Biomedical Imaging and Bioengineering from the National Institutes of Health: Quantum Award Phase I R01, EB008004-01 (DB), and Quantum Award: Implementation Phase II-1U01EB012487-0 (DB). We thank Bryan Lynch from MicroMed Cardiovascular, Inc. for providing VADs for this study.

References

[1] Go, A. S., Mozaffarian, D., Roger, V. L., Benjamin, E. J., Berry, J. D., Borden, W. B., Bravata, D. M., Dai, S., Ford, E. S., Fox, C. S., Franco, S., Fullerton, H. J., Gillespie, C., Hailpern, S. M., Heit, J. A., Howard, V. J., Huffman, M. D., Kissela, B. M., Kittner, S. J., Lackland, D. T., Lichtman, J. H., Lisabeth, L. D., Magid, D., Marcus, G. M., Marelli, A., Matchar, D. B., Mcguire, D. K., Mohler, E. R., Moy, C. S., Mussolino, M. E., Nichol, G., Paynter, N. P., Schreiner, P. J., Sorlie, P. D., Stein, J., Turan, T. N., Virani, S. S., Wong, N. D., Woo, D., and Turner, M. B., 2013, "Heart Disease and Stroke Statistics–2013 Update: A Report from the American Heart Association," Circulation, **127**(1), pp. e6–e245.

[2] Kurihara, C., Ono, M., Nishimura, T., Nawata, K., Kinoshita, O., Hisagi, M., Motomura, N., and Kyo, S., 2011, "Prolonged Biventricular Assist Device Support as a Bridge to Heart Transplantation," Int. J. Artif. Organs, **14**(4), pp. 367–370.

[3] Copeland, J. G., Copeland, H., Gustafson, M., Mineburg, N., Covington, D., Smith, R. G., and Friedman, M., 2012, "Experience With More Than 100 Total Artificial Heart Implants," J Thorac. Cardiovasc. Surg., **143**(3), pp. 727–734.

[4] Srtr, 2011, Optn/Srtr 2011, "Annual Data Report: Heart." Available at: http://srtr.transplant.hrsa.gov/annual_reports/2011/

[5] Kirklin, J. K., Naftel, D. C., Kormos, R. L., Stevenson, L. W., Pagani, F. D., Miller, M. A., Baldwin, J. T., and Young, J. B., 2012, "The Fourth Intermacs Annual Report: 4,000 Implants and Counting," J. Heart Lung Transplant, **31**(2), pp. 117–126.

[6] Slaughter, M. S., Rogers, J. G., Milano, C. A., Russell, S. D., Conte, J. V., Feldman, D., Sun, B., Tatooles, A. J., Delgado, R. M. III, Long, J. W., Wozniak, T. C., Ghumman, W., Farrar, D. J., and Frazier, O. H., 2009, "Advanced Heart Failure Treated With Continuous-Flow Left Ventricular Assist Device," N. Engl. J. Med., **361**(23), pp. 2241–2251.

[7] Lahpor, J. R., 2009, "State of the Art: Implantable Ventricular Assist Devices," Curr. Opin. Organ Transplant, **14**(5), pp. 554–559.

[8] Carrel, T., Englberger, L., Martinelli, M. V., Takala, J., Boesch, C., Sigurdadottir, V., Gygax, E., Kadner, A., and Mohacsi, P., 2012, "Continuous Flow Left Ventricular Assist Devices: A Valid Option for Heart Failure Patients," Swiss Med. Wkly., **142**, pp. w13701.

[9] Heilmann, C., Geisen, U., Benk, C., Berchtold-Herz, M., Trummer, G., Schlensak, C., Zieger, B., and Beyersdorf, F., 2009, "Haemolysis in Patients With Ventricular Assist Devices: Major Differences Between Systems," Eur. J. Cardiothorac. Surg., 36**36**, pp. 580–584.

[10] Snyder, T. A., Watach, M. J., Litwak, K. N., and Wagner, W. R., 2002, "Platelet Activation, Aggregation, and Life Span in Calves Implanted With Axial Flow Ventricular Assist Devices," Ann. Thorac. Surg., **73**, pp. 1933–1938.

[11] Girdhar, G., Xenos, M., Alemu, Y., Chiu, W. C., Lynch, B. E., Jesty, J., Einav, S., Slepian, M. J., and Bluestein, D., 2012, "Device Thrombogenicity Emulation: A Novel Method for Optimizing Mechanical Circulatory Support Device Thromboresistance," PLoS ONE, **7**(3), p. e32463.

[12] Mokadam, N. A., Andrus, S., and Ungerleider, A., 2011, "Thrombus Formation in a Heartmate Ii," Eur. J. Cardiothorac. Surg., **39**(3), p. 414.

[13] Meyer, A. L., Kuehn, C., Weidemann, J., Malehsa, D., Bara, C., Fischer, S., Haverich, A., and Struber, M., 2008, "Thrombus Formation in a Heartmate Ii Left Ventricular Assist Device," J. Thorac. Cardiovasc. Surg., **135**(1), pp. 203–204.

[14] Najib, M. Q., Wong, R. K., Pierce, C. N., Devaleria, P. A., and Chaliki, H. P., 2012, "An Unusual Presentation of Left Ventricular Assist Device Thrombus," Eur. Heart J. Cardiovasc. Imaging, **13**(6), p. 532.

[15] Pappalardo, F., Scandroglio, A. M., Potapov, E., Stepanenko, A., Maj, G., Krabatsch, T., Zangrillo, A., Koster, A., and Hetzer, R., 2012, "Argatroban Anticoagulation for Heparin Induced Thrombocytopenia in Patients With Ventricular Assist Devices," Minerva Anestesiol., **78**(3), pp. 330–335.

[16] Geisen, U., Heilmann, C., Beyersdorf, F., Benk, C., Berchtold-Herz, M., Schlensak, C., Budde, U., and Zieger, B., 2008, "Non-Surgical Bleeding in Patients With Ventricular Assist Devices Could Be Explained by Acquired Von Willebrand Disease," Eur. J. Cardiothorac. Surg., **33**(4), pp. 679–684.

[17] Meyer, A. L., Malehsa, D., Bara, C., Budde, U., Slaughter, M. S., Haverich, A., and Strueber, M., 2010, "Acquired Von Willebrand Syndrome in Patients With an Axial Flow Left Ventricular Assist Device," Circ. Heart Fail, **3**(6), pp. 675–681.

[18] Malehsa, D., Meyer, A. L., Bara, C., and Struber, M., 2009, "Acquired Von Willebrand Syndrome after Exchange of the Heartmate Xve to the Heartmate Ii Ventricular Assist Device," Eur. J. Cardiothorac. Surg., **35**(6), pp. 1091–1093.

[19] Alemu, Y., Girdhar, G., Xenos, M., Sheriff, J., Jesty, J., Einav, S., and Bluestein, D., 2010, "Design Optimization of a Mechanical Heart Valve for Reducing Valve Thrombogenicity-A Case Study With Ats Valve," ASAIO J., **56**(5), pp. 389–396.

[20] Bluestein, D., Einav, S., and Slepian, M. J., 2013, "Device Thrombogenicity Emulation: A Novel Methodology for Optimizing the Thromboresistance of Cardiovascular Devices," J. Biomech., **46**(2), pp. 338–344.

[21] Xenos, M., Girdhar, G., Alemu, Y., Jesty, J., Slepian, M., Einav, S., and Bluestein, D., 2010, "Device Thrombogenicity Emulator (Dte)–Design Optimization Methodology for Cardiovascular Devices: A Study in Two Bileaflet Mhv Designs," J. Biomech., **43**(12), pp. 2400–2409.

[22] Stern, D. R., Kazam, J., Edwards, P., Maybaum, S., Bello, R. A., D'alessandro, D. A., and Goldstein, D. J., 2010, "Increased Incidence of Gastrointestinal Bleeding Following Implantation of the Heartmate Ii Lvad," J. Card. Surg., **25**(3), pp. 352–356.

[23] Sponga, S., Nalli, C., Casonato, A., and Charbonneau, E., 2012, "Severe Upper Gastrointestinal Bleeding in Heartmate Ii Induced by Acquired Von Willebrand Deficiency: Anticoagulation Management," Ann. Thorac. Surg., **94**(2), pp. e41–e43.

[24] Park, S. J., Milano, C. A., Tatooles, A. J., Rogers, J. G., Adamson, R. M., Steidley, D. E., Ewald, G. A., Sundareswaran, K. S., Farrar, D. J., Slaughter, M. S.,

and Heartmate, I. I. C. I., 2012, "Outcomes in Advanced Heart Failure Patients With Left Ventricular Assist Devices for Destination Therapy," Circ. Heart Fail, **5**(2), pp. 241–248.
[25] Bluestein, D., Rambod, E., and Gharib, M., 2000, "Vortex Shedding as a Mechanism for Free Emboli Formation in Mechanical Heart Valves," ASME J. Biomech. Eng., **122**(2), pp. 125–134.
[26] Bludszuweit, C., 1995, "Three-Dimensional Numerical Prediction of Stress Loading of Blood Particles in a Centrifugal Pump," Artif. Organs, **19**(7), pp. 590–596.
[27] Bludszuweit, C., 1995, "Model for a General Mechanical Blood Damage Prediction," Artif. Organs, **19**(7), pp. 583–589.
[28] Arora, D., Behr, M., and Pasquali, M., 2004, "A Tensor-Based Measure for Estimating Blood Damage," Artif. Organs, **28**(11), pp. 1002–1015.
[29] Alemu, Y., and Bluestein, D., 2007, "Flow-Induced Platelet Activation and Damage Accumulation in a Mechanical Heart Valve: Numerical Studies," Artif. Organs, **31**(9), pp. 677–688.
[30] Capoccia, M., Bowles, C. T., Sabashnikov, A., and Simon, A., 2013, "Recurrent Early Thrombus Formation in Heartmate Ii Left Ventricular Assist Device" J. Investig. Med. High Impact Case Reports, **1**(2), pp. 1–3.
[31] Jesty, J., and Bluestein, D., 1999, "Acetylated Prothrombin as a Substrate in the Measurement of the Procoagulant Activity of Platelets: Elimination of the Feedback Activation of Platelets by Thrombin," Anal. Biochem., **272**(1), pp. 64–70.